

Swap Monte Carlo for diatomic molecules

Till Böhmer,^{*} Jeppe C. Dyre,[†] and Lorenzo Costigliola[‡]
*Glass and Time, IMFUFA, Department of Science and Environment,
Roskilde University, P.O. Box 260, DK-4000 Roskilde, Denmark*
(Dated: April 22, 2025)

In recent years the Swap Monte Carlo algorithm has led to remarkable progress in equilibrating supercooled model liquids at low temperatures. Applications have so far been limited to systems composed of spherical particles, however, whereas most real-world supercooled liquids are molecular. We here introduce a simple size-polydisperse molecular model that allows for efficient thermal equilibration *in silico* with the Swap Monte Carlo method, resulting in an estimated speedup of $10^3 - 10^6$ at moderate polydispersity (5-10%). Despite being polydisperse, the model exhibits little difference between the size-resolved orientational time-autocorrelation functions. Our results demonstrate the possibility of designing molecular models that can be simulated close to the calorimetric glass transition.

When a liquid is cooled fast enough to avoid crystallization, the viscosity increases by typically a factor of 10^{15} before the system solidifies at the glass transition [1–10]. The relaxation time increases by a similar factor, and the glass state is arrived at when the equilibration time exceeds the cooling time. Glass-forming liquids continue to attract attention from the physics, chemistry, and material-science communities because fundamental scientific problems remain unsolved, e.g.: What controls the extreme slowing down? What causes the ubiquitous deviations from single-exponential relaxation? How to describe the physical aging taking place below the glass transition? To elucidate such challenging questions it is imperative to have realistic model liquids that can be simulated in ultraviscous conditions.

This millennium has witnessed unprecedented advances in glass science that give access to data previously thought to be far beyond reach. Ultrastable glasses have made possible the production of glasses, which it would take thousands of years to make by cooling from the melt [11]. There have also been tremendous advances in computer simulations, both from hardware improvements including the use of graphics processing units (GPUs) [12] and from algorithmic advances. For systems of point particles Swap Monte-Carlo (MC) algorithms now allow for numerically generating ultrastable glasses, as well as equilibrated extremely viscous liquid states [13–21]. This and similar approaches [22–24] are continuously being improved in a field of rapid development. Most recently ultrastable glasses have been achieved by randomly bonding particle pairs resulting in a mixture of atoms and polydisperse binary molecules [25], by homogenizing the local virial stress to produce ultrastable glasses in simulations [26], and in numerical studies of metallic glass formers [20, 27].

The Swap MC method allows for unphysical moves where randomly chosen particles are swapped. This trick gained renewed attention when Ninarello *et al.* in 2017 introduced a continuous size-polydisperse system of spherical particles interacting via a soft repulsive pair

potential [18]. This model proved to be highly stable against crystallization and demixing, making it ideal for equilibrating low-temperature supercooled liquid configurations via Swap MC [18, 19]. By alternating standard MC displacement moves with particle swaps, the dynamics is accelerated by up to ten orders of magnitude, allowing one to obtain equilibrium configurations below the experimental glass-transition temperature [18]. This model has become a standard system for exploring the physics of deeply supercooled liquids, and studies of it have enabled advances [12] in the understanding of glass physics in relation to, e.g., dynamic heterogeneity [28, 29], dynamic facilitation [30–32], yielding [33–38], cooperativity [39], vibrational properties [40, 41], and physical aging [42–44].

Despite its success, Swap MC has so far only been applied to point-particle model liquids. Many real-world supercooled liquids and glasses are composed of molecules, however, and a substantial body of experimental research has documented the distinctive physics of supercooled molecular liquids [8, 45–47]. This paper introduces a minimal molecular model, which can be equilibrated efficiently via Swap MC at the molecular level. This allows one to obtain equilibrium configurations near the experimental glass-transition temperature at a reasonable computational cost, thus providing a first step in connecting the world of experimental ultrastable molecular glasses with that of Swap numerical studies.

For a model to capture faithfully the physics of real-world supercooled molecular liquids, size polydispersity cannot be allowed. On the other hand, efficient equilibration via Swap MC relies on introducing polydispersity. That this can lead to significant issues was recently pointed out by Pihlajamaa *et al.* [48] for the above-mentioned “standard” Swap MC system [18] with $\delta \approx 23\%$ polydispersity (defined as variance over squared average). At deeply supercooled temperatures, the smallest and largest particles exhibit drastically different behavior; thus their average relaxation times differ up to a factor of 50 and they moreover exhibit markedly differ-

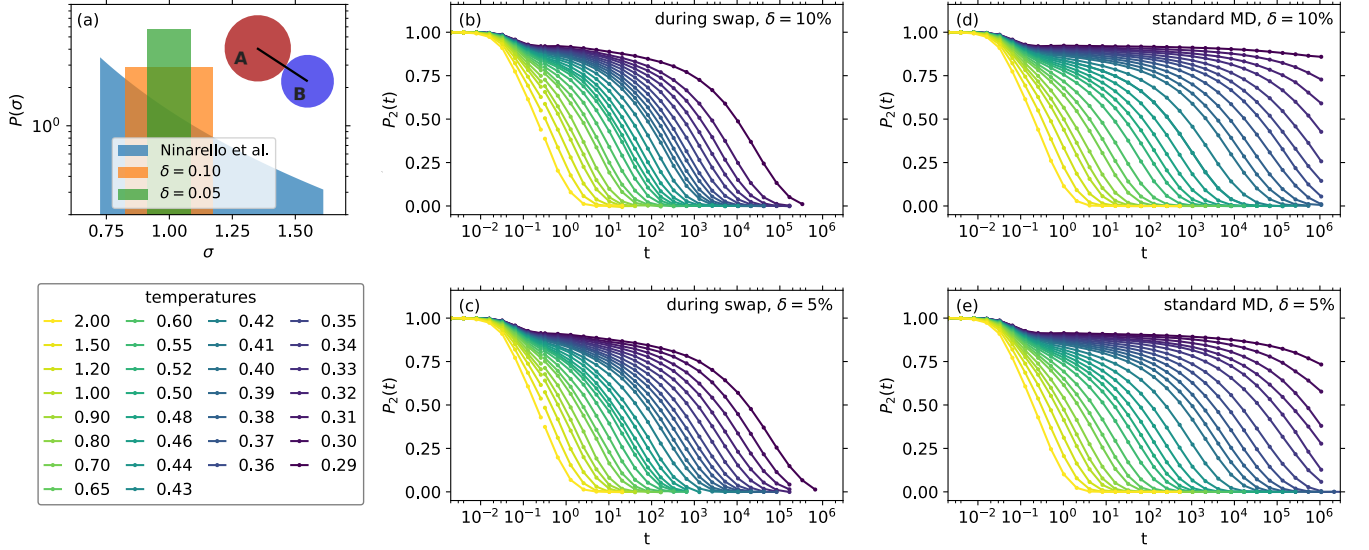


FIG. 1. (a) Particle-size distribution for the investigated systems with polydispersities $\delta = 5\%$ and $\delta = 10\%$. For comparison, we include the distribution for the “standard” Swap MC system [18] with $\delta \approx 23\%$ (blue curve). Panels (b)-(e) show orientational time-autocorrelation functions $P_2(t)$ (Eq. (2)) during Swap MC (b,c) and standard MD simulation (d,e) for various temperatures and for the two polydispersities $\delta = 5\%$ (upper panels) and $\delta = 10\%$ (lower panels). Corresponding plots for the intermediate scattering function and the first-order orientational time-autocorrelation function can be found in the Appendix.

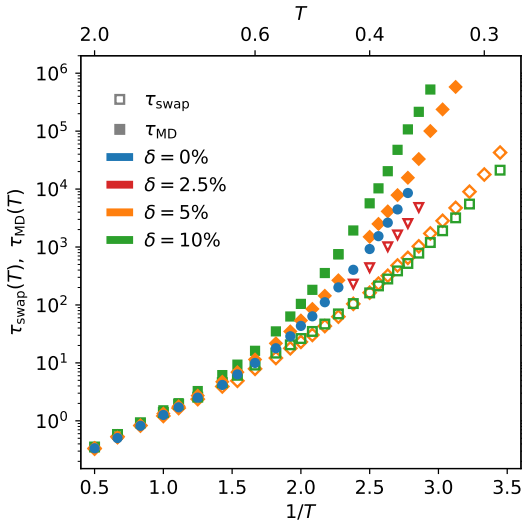


FIG. 2. Orientational relaxation times τ_{Swap} (open symbols) and τ_{MD} (full symbols) during Swap and standard MD simulations, respectively, plotted as function of inverse temperature. The blue symbols are data for the monodisperse ASD system ($\delta = 0\%$).

ent motion mechanisms. To mitigate such polydispersity-induced effects, we only simulated polydispersities up to 10%. As shown below, Swap MC for our molecular model remains efficient even for $\delta = 5\%$. We show that at such low levels the influence of polydispersity on the dynamics is minimal, demonstrating the viability of our model as a realistic minimal model of deeply supercooled molecular

liquids.

We simulated monodisperse and polydisperse systems composed of asymmetric dumbbell (ASD) molecules at the molecular (number) density $\rho = 0.932$ under periodic boundary conditions. Each molecule consists of two particles, denoted as A and B (Fig. 1(a)), with masses $m_A = 1$ and $m_B = 0.195$. Particles A and B of the same molecule interact via a harmonic bond of equilibrium length $l = 0.584$ and spring constant $k = 3000$. The intermolecular interactions are modeled using the Lennard-Jones (LJ) potential, i.e., the potential between particles i and j at distance $r = |\mathbf{r}_i - \mathbf{r}_j|$ is given by

$$v_{ij}(r) = 4\epsilon_{ij} \left[\left(\frac{r}{\sigma_{ij}} \right)^{-12} - \left(\frac{r}{\sigma_{ij}} \right)^{-6} \right]. \quad (1)$$

The pair potential is cut at $r = 2.5\sigma_{ij}$ using the shifted-force method [49, 50].

The size and energy parameters σ_{ij} and ϵ_{ij} follow the standard Lorentz-Berthelot mixing rules, $\sigma_{ij} = (\sigma_i + \sigma_j)/2$ and $\epsilon_{ij} = \sqrt{\epsilon_i \epsilon_j}$, in which σ_i and ϵ_i denote the size and energy parameter of particle i , respectively. The particle sizes are given by $\sigma_A = 1$ and $\sigma_B = 0.788\sigma_A$ for the monodisperse system. Polydispersity is introduced such that the A and B particles' sizes of the same molecule are scaled by the same amount. Thus the B particle is slaved to that of the same-molecule A particle according to $\sigma_B = 0.788\sigma_A$, leaving the harmonic bond length unchanged (note that this lowers the effective molecular size polydispersity compared to that of the A and B particles). The characteristic energies of A and B particles

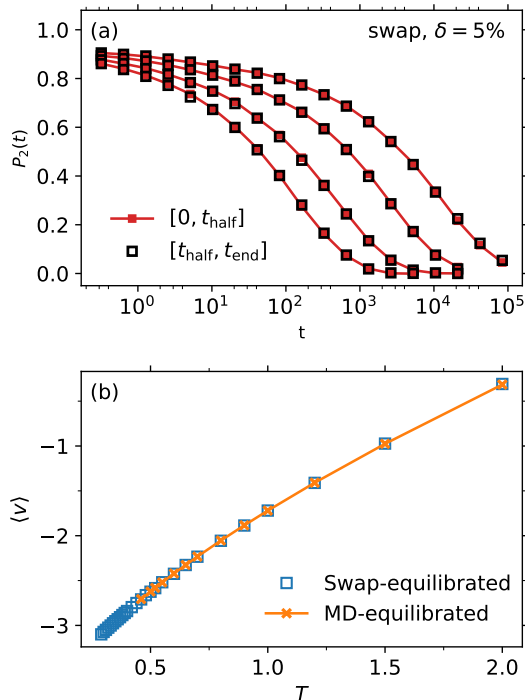


FIG. 3. Confirming that the configurations obtained from the equilibration procedure using Swap are in equilibrium. (a) illustrates the absence of aging by showing that orientational time-autocorrelation data during Swap averaged over the first half (red symbols) and the second half (black symbols) of the simulation are identical. We show selected data for the temperatures $T = 0.31, 0.34, 0.38$ and 0.42 . (b) Average per-particle potential energy $\langle u \rangle$ as function of temperature. The data for Swap-equilibrated configurations (blue symbols) extend smoothly to lower temperatures the data of the MD-equilibrated configurations (orange data).

are fixed to $\epsilon_A = 1$ and $\epsilon_B = 0.117$.

We study systems with different degrees of polydispersity by choosing σ_A to be uniformly distributed as $\sigma_A \in [1 - \Delta, 1 + \Delta]$ with $\Delta = \sqrt{12}\delta/2$, which for 5% and 10% polydispersity corresponds to $\Delta = 0.087$ and $\Delta = 0.173$, respectively. Randomly drawing a value σ_A from the distribution for each molecule could lead to substantial finite size effects by sampling the distribution inaccurately [51]. Therefore, we sampled the distribution inspired by the procedure of K uchler and Horbach [21, 51] by defining 500 different types of molecules, whose σ_A -values are equidistantly spaced within $[1 - \Delta, 1 + \Delta]$. There are thus four molecules of each size in our system consisting of 2000 molecules.

Two kinds of simulations were performed: 1) Standard NVT (MD) simulations employing the time step $\Delta t = 0.002$ and a Nos e-Hoover thermostat with relaxation time 0.2. The MD units refer to the size and energy of A particles in the monodisperse model. 2) Swap MC simulations, where we alternate between short segments

of NVT simulations (for $t = 0.32$ each, with $\Delta t = 0.005$) and $2N$ consecutive attempts of swapping the parameters σ_A (and, therefore, also σ_B) of randomly chosen pairs of molecules. Each swap attempt is accepted with a probability according to the Metropolis rule, resulting in acceptance rates of 15-30% (Appendix). To obtain equilibrium configurations, we performed standard MD simulations for at least $500\tau_{\text{MD}}$ at higher temperatures ($T \geq 0.42$), and Swap MC for at least $50-200\tau_{\text{swap}}$ at low temperatures ($50\tau_{\text{swap}}$ is used for the three lowest studied temperatures). Here, τ_{MD} and τ_{swap} denote the orientational relaxation time during standard MD and Swap, respectively. That configurations are truly in equilibrium is confirmed by the absence of aging (see below). We did not observe any signs of crystallization or structure formation in any simulations.

All simulations were performed using RUMDPY, an in-development Python simulation package employing similar optimizations as RUMD [52] to enable GPU-accelerated MD simulations [53]. Swap moves were implemented on the CPU, however, as they do not benefit from GPU parallelization. Since particle positions remain unchanged during a series of swap attempts, the neighbor list for interaction calculations can be reused from the preceding MD sequence, allowing for efficient GPU calculation.

Fig. 1 illustrates the molecular reorientation dynamics for $\delta = 5\%$ and 10% polydispersity at various temperatures for (b,c) Swap and (d,e) standard MD simulations, quantified via the single-molecule second-order orientational time-autocorrelation function

$$P_2(t) = \langle 3 \cos^2 \Theta(t) - 1 \rangle / 2. \quad (2)$$

Here, $\Theta(t)$ is the angle between the molecule's orientation at time 0 and time t , and $\langle \dots \rangle$ indicates a moving time-average and average over all molecules. In case of Swap, t reflects the cumulative duration of the short MD sequences in-between the molecule swaps.

For both Swap and standard MD dynamics, the time-autocorrelation functions exhibit a characteristic two-step decay: First, a low-amplitude short-time decay (relaxation time $\tau_0 \approx 10^{-1}$) corresponding to the molecules exploring local cages, followed by a long-time decay associated with structural relaxation due to breaking of the local cages. The structural relaxation is significantly accelerated during Swap, especially at low temperatures. The equilibrium data at temperatures $T \lesssim 0.38$ shown in Fig. 1(d,e) could only be obtained by employing Swap for preparing the initial configurations. Achieving equivalent equilibration using standard MD would require computational times ranging from months to several years, even using GPU-based software [52]. Equivalent conclusions are drawn from the self-intermediate scattering function quantifying translational dynamics, or from a different orientational autocorrelation function (Appendix).

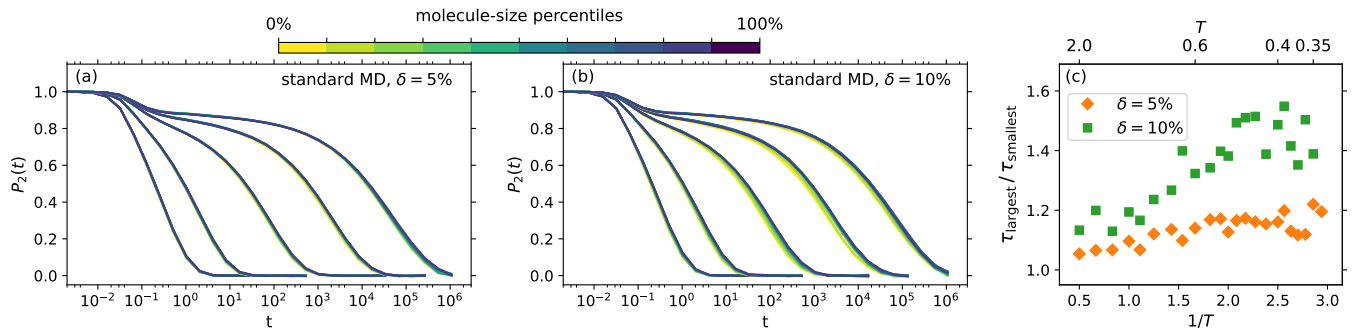


FIG. 4. (a) and (b): Molecule-size resolved orientational time-autocorrelations from standard MD simulations for $\delta = 5\%$ and 10% . The colors represent data obtained for different 10%-percentiles of the molecule-size distribution (see the color bar). The shown temperatures are $T = 2.0, 0.9, 0.50, 0.40, 0.35$ for $\delta = 5\%$ and $T = 2.0, 0.9, 0.52, 0.42, 0.37$ for $\delta = 10\%$. (c) The quotient $\tau_{\text{smallest}}/\tau_{\text{largest}}$ between the relaxation times found for 10% smallest and 10% largest molecules as a function of temperature.

Figure 2 summarizes the speedup achieved by Swap relative to standard MD by showing the respective orientational relaxation times τ_{swap} (open symbols) and τ_{MD} (full symbols) as functions of the inverse temperature. Relaxation times are defined via the condition $P_2(\tau) = 1/e$. The speedup provided by Swap increases markedly with decreasing temperature. While it decreases with decreasing polydispersity, it remains significant even for $\delta = 5\%$, whereas $\delta = 2.5\%$ proves insufficient to yield a meaningful speedup.

To estimate the maximum speedup achieved in this study, we examine τ_{swap} and τ_{MD} at the lowest accessible temperature, $T = 0.29$. Since $\tau_{\text{MD}}(T = 0.29)$ exceeds the time scale resolvable by standard MD simulations, we extrapolate it using established models for the temperature-dependence of relaxation times. We applied both the Vogel-Fulcher-Tamann (VFT) equation [54] and a parabolic law [55] (which yield different predictions), leading to a range of values. For $\delta = 10\%$, we find a maximum speedup $\tau_{\text{MD}}(T = 0.29)/\tau_{\text{swap}}(T = 0.29)$ of approximately $10^4 - 10^6$; for $\delta = 5\%$ the range is approximately $10^3 - 10^4$ for. Using τ_0 defined above and following the criterion $\tau_{\text{MD}}(T_g)/\tau_0 = 10^{12}$ we estimate the experimental glass-transition temperatures to be $T_g(\delta = 10\%) \approx 0.265 - 0.285$ and $T_g(\delta = 5\%) \approx 0.250 - 0.270$. This method for estimating T_g for the molecular models is the same used for the standard Swap model [18, 19].

In addition to the data for 5% and 10% polydispersity, we include in Fig. 2 also the standard MD relaxation times of the monodisperse system (blue symbols). There is a mild dependence of $\tau_{\text{MD}}(T)$ on the polydispersity, i.e., the relaxation time at a given temperature increases slightly with increasing δ . A similar effect was reported by Parmar *et al.* for a modified version of the Kob-Andersen binary LJ mixture [20].

To confirm that the configurations obtained via Swap are in thermal equilibrium, we demonstrate in Fig. 3(a) the absence of any physical aging. For a system that is not in equilibrium, one will observe an explicit de-

pendence of the time-resolved autocorrelation function $C(t_1, t_2)$ on the waiting time t_1 , such that $C(t_1, t_1 + t)$ depends on both t_1 and t [56, 57]. This behavior is not observed for the Swap-equilibrated configurations; thus $P_2(t)$ averaged over the first half of the simulation $t_1 \in [0, t_{1/2}]$ (red symbols) is indistinguishable from that averaged over the second half $t_1 \in [t_{1/2}, t_{\text{final}}]$ (black symbols). Another confirmation that the systems are in thermal equilibrium involves monitoring the average per-particle potential energy, which is shown in Fig 3(b) for Swap- (blue) and MD-equilibrated (orange) configurations as a function of temperature. The data for Swap-equilibrated configurations extend the data of the MD-equilibrated configurations to lower temperatures without any noticeable kink or bend, as would be observed if Swap did not reach equilibrium [58].

This study has introduced a simple molecular model system that captures the essential features of real-world deeply supercooled molecular liquids, like the existence of molecular bonds, anisotropic intermolecular interactions and rotational degrees of freedom. In terms of the accessible temperature range, Fig. 2 confirms that the equilibrium configurations can be obtained at temperatures comparable to those studied in typical experiments [45, 47], i.e., $\tau_{\text{MD}}/\tau_0 \sim 10^6 - 10^{12}$ corresponding to real times approaching seconds. An important aspect to consider is the role of polydispersity, which is absent in a real molecular liquid. Polydispersity is not expected to significantly alter the underlying physics if the smallest and the largest molecules in the system exhibit the same or very similar dynamics. To test this we study in Figs 4(a) and (b) the molecule-size resolved reorientation dynamics. This is done by plotting $P_2(t)$ for different 10%-percentiles of the molecule-size distribution at selected temperatures. Clearly, the smallest and the largest molecules behave similarly. This is confirmed in (c), which shows the quotient of relaxation times of the 10% largest and the 10% smallest molecules. While there is an increase upon cooling, the ratio eventually

saturates and does not exceed 1.2 and 1.5 for 5% and 10% polydispersity, respectively. This is in stark contrast to $\tau_{\text{largest}}/\tau_{\text{smallest}} \approx 50$ found for point-particle systems with larger polydispersity [48]. We conclude that the proposed ASD system with polydispersity around 5-10% can serve as a minimal model for real-life deeply supercooled molecular liquids.

The presented procedure can be readily extended to more complex molecular models. However, the efficiency of Swap equilibration is likely to decrease with increasing complexity. This is because larger molecules require larger available volume to relax, which can no longer be provided by swapping the sizes of atoms. Nevertheless, the above procedure should be applicable to trimer systems. Exploring this direction of research will be the subject of future work.

In summary, we have introduced a Swap MC procedure for efficiently generating equilibrium supercooled liquid configurations of a simple diatomic molecular model *in silico*, which allows for reaching temperatures approaching that of the experimental glass transition. This was achieved using a system composed of dimers with a minor size polydispersity at the molecule level, in conjunction with an algorithm alternating between swapping the sizes of randomly chosen pairs of molecules and short NVT simulations. By analyzing relaxation times for the dynamics with and without swaps, the procedure was found to accelerate equally the rotational and translational (Appendix) degrees of freedom. We explored the acceleration of dynamics in the low-polydispersity limit and found that Swap remains efficient down to 5% polydispersity. Analyzing the molecule-size-resolved dynamics, we showed that polydispersity in the 5–10% range hardly alters the qualitative physical behavior of the system, which runs contrary to what applies for point-particle systems of higher polydispersity [48]. These findings suggest that the introduced model is a promising candidate for future studies of deeply supercooled molecular liquids – in particular for comparing to the large body of experimental data, e.g., on the dielectric relaxation of molecular glass formers [8, 46, 47].

This work was supported by the VILLUM Foundation’s *Matter* grant (VIL16515).

* till.boehmer@pkm.tu-darmstadt.de

† dyre@ruc.dk

‡ lorenzo.costigliola@gmail.com

- [1] W. Kauzmann, The nature of the glassy state and the behavior of liquids at low temperatures, *Chem. Rev.* **43**, 219 (1948).
 [2] G. Harrison, *The Dynamic Properties of Supercooled Liquids* (Academic, New York, 1976).
 [3] C. A. Angell, Formation of glasses from liquids and biopolymers, *Science* **267**, 1924 (1995).

- [4] P. G. Debenedetti and F. H. Stillinger, Supercooled liquids and the glass transition, *Nature* **410**, 259 (2001).
 [5] J. C. Dyre, The glass transition and elastic models of glass-forming liquids, *Rev. Mod. Phys.* **78**, 953 (2006).
 [6] L. Berthier and G. Biroli, Theoretical perspective on the glass transition and amorphous materials, *Rev. Mod. Phys.* **83**, 587 (2011).
 [7] G. L. Hunter and E. R. Weeks, The physics of the colloidal glass transition, *Rep. Prog. Phys.* **75**, 066501 (2012).
 [8] R. Richert, Supercooled liquids and glasses by dielectric relaxation spectroscopy, *Adv. Chem. Phys.* **156**, 101 (2015).
 [9] J. C. Mauro, *Materials Kinetics: Transport and Rate Phenomena* (Elsevier, Amsterdam, Netherlands, 2021).
 [10] C. Alba-Simionesco and G. Tarjus, A perspective on the fragility of glass-forming liquids, *J. Non-Cryst. Solids X* **14**, 100100 (2022).
 [11] M. D. Ediger, Perspective: Highly stable vapor-deposited glasses, *J. Chem. Phys.* **147**, 210901 (2017).
 [12] L. Berthier and D. R. Reichman, Modern computational studies of the glass transition, *Nat. Phys. Rev.* **5**, 102 (2023).
 [13] T. S. Grigera and G. Parisi, Fast Monte Carlo algorithm for supercooled soft spheres, *Phys. Rev. E* **63**, 045102 (2001).
 [14] Y. Brumer and D. R. Reichman, Numerical investigation of the entropy crisis in model glass formers, *J. Phys. Chem. B* **108**, 6832 (2004).
 [15] L. A. Fernández, V. Martín-Mayor, and P. Verrocchio, Critical behavior of the specific heat in glass formers, *Phys. Rev. E* **73**, 020501 (2006).
 [16] L. A. Fernández, V. Martín-Mayor, and P. Verrocchio, Phase diagram of a polydisperse soft-spheres model for liquids and colloids, *Phys. Rev. Lett.* **98**, 085702 (2007).
 [17] A. Cavagna, T. S. Grigera, and P. Verrocchio, Dynamic relaxation of a liquid cavity under amorphous boundary conditions, *J. Chem. Phys.* **136**, 204502 (2012).
 [18] A. Ninarello, L. Berthier, and D. Coslovich, Models and algorithms for the next generation of glass transition studies, *Phys. Rev. X* **7**, 021039 (2017).
 [19] L. Berthier, E. Flenner, C. J. Fullerton, C. Scalliet, and M. Singh, Efficient swap algorithms for molecular dynamics simulations of equilibrium supercooled liquids, *J. Stat. Mech.:Theory Exp.* **2019**, 064004 (2019).
 [20] A. D. S. Parmar, M. Ozawa, and L. Berthier, Ultrastable metallic glasses in silico, *Phys. Rev. Lett.* **125**, 085505 (2020).
 [21] N. Küchler and J. Horbach, Understanding the swap Monte Carlo algorithm in a size-polydisperse model glass-former, *Phys. Rev. E* **108**, 024127 (2023).
 [22] R. Yamamoto and W. Kob, Replica-exchange molecular dynamics simulation for supercooled liquids, *Phys. Rev. E* **61**, 5473 (2000).
 [23] K. Hukushima and K. Nemoto, Exchange Monte Carlo method and application to spin glass simulations, *J. Phys. Soc. Jpn.* **65**, 1604 (1996).
 [24] K. Shiraishi, H. Mizuno, and A. Ikeda, Johari – Goldstein β relaxation in glassy dynamics originates from two-scale energy landscape, *PNAS* **120**, e2215153120 (2023).
 [25] M. Ozawa, Y. Iwashita, W. Kob, and F. Zamponi, Creating bulk ultrastable glasses by random particle bonding, *Nat. Comm.* **14**, 113 (2023).
 [26] F. Leoni, J. Russo, F. Sciortino, and T. Yanagishima,

- Generating ultrastable glasses by homogenizing the local virial stress, *Phys. Rev. Lett.* **134**, 128201 (2025).
- [27] A. D. S. Parmar, B. Guiselin, and L. Berthier, Stable glassy configurations of the Kob–Andersen model using swap Monte Carlo, *J. Chem. Phys.* **153**, 134505 (2020).
- [28] L. Berthier, Self-induced heterogeneity in deeply supercooled liquids, *Phys. Rev. Lett.* **127**, 088002 (2021).
- [29] G. Jung, G. Biroli, and L. Berthier, Dynamic heterogeneity at the experimental glass transition predicted by transferable machine learning, *Phys. Rev. B* **109**, 064205 (2024).
- [30] C. Scalliet, B. Guiselin, and L. Berthier, Thirty milliseconds in the life of a supercooled liquid, *Phys. Rev. X* **12**, 041028 (2022).
- [31] B. Guiselin, C. Scalliet, and L. Berthier, Microscopic origin of excess wings in relaxation spectra of supercooled liquids, *Nat. Phys.* **18**, 468 (2022).
- [32] C. Herrero and L. Berthier, Direct numerical analysis of dynamic facilitation in glass-forming liquids, *Phys. Rev. Lett.* **132**, 258201 (2024).
- [33] M. Ozawa, L. Berthier, G. Biroli, A. Rosso, and G. Tarjus, Random critical point separates brittle and ductile yielding transitions in amorphous materials, *Proc. Natl. Acad. Sci. U.S.A.* **115**, 6656 (2018).
- [34] D. Richard, M. Ozawa, S. Patinet, E. Stanifer, B. Shang, S. A. Ridout, B. Xu, G. Zhang, P. K. Morse, J.-L. Barrat, L. Berthier, M. L. Falk, P. Guan, A. J. Liu, K. Martens, S. Sastry, D. Vandembroucq, E. Lerner, and M. L. Manning, Predicting plasticity in disordered solids from structural indicators, *Phys. Rev. Mater.* **4**, 113609 (2020).
- [35] M. Singh, M. Ozawa, and L. Berthier, Brittle yielding of amorphous solids at finite shear rates, *Phys. Rev. Mater.* **4**, 025603 (2020).
- [36] W.-T. Yeh, M. Ozawa, K. Miyazaki, T. Kawasaki, and L. Berthier, Glass stability changes the nature of yielding under oscillatory shear, *Phys. Rev. Lett.* **124**, 225502 (2020).
- [37] K. Lamp, N. K uchler, and J. Horbach, Brittle yielding in supercooled liquids below the critical temperature of mode coupling theory, *J. Chem. Phys.* **157**, 034501 (2022).
- [38] M. Ozawa, L. Berthier, G. Biroli, and G. Tarjus, Rare events and disorder control the brittle yielding of well-annealed amorphous solids, *Phys. Rev. Res.* **4**, 023227 (2022).
- [39] M. Pica Ciamarra, W. Ji, and M. Wyart, Local vs. cooperative: Unraveling glass transition mechanisms with seer, *Proc. Natl. Acad. Sci. U.S.A.* **121**, e2400611121 (2024).
- [40] L. Wang, A. Ninarello, P. Guan, L. Berthier, G. Szamel, and E. Flenner, Low-frequency vibrational modes of stable glasses, *Nat. Comm.* **10**, 26 (2019).
- [41] D. Xu, S. Zhang, H. Tong, L. Wang, and N. Xu, Low-frequency vibrational density of states of ordinary and ultra-stable glasses, *Nat. Comm.* **15**, 1424 (2024).
- [42] C. Herrero, C. Scalliet, M. D. Ediger, and L. Berthier, Two-step devitrification of ultrastable glasses, *Proc. Natl. Acad. Sci. U.S.A.* **120**, e2220824120 (2023).
- [43] R. N. Chacko, F. m. c. P. Landes, G. Biroli, O. Dauchot, A. J. Liu, and D. R. Reichman, Dynamical facilitation governs the equilibration dynamics of glasses, *Phys. Rev. X* **14**, 031012 (2024).
- [44] C. Herrero, M. D. Ediger, and L. Berthier, Front propagation in ultrastable glasses is dynamically heterogeneous, *J. Chem. Phys.* **159**, 114504 (2023).
- [45] P. Lunkenheimer, U. Schneider, R. Brand, and A. Loidl, Glassy dynamics, *Contemp. Phys.* **41**, 15 (2000).
- [46] F. Kremer and A. Loidl, *The scaling of relaxation processes* (Springer, 2018).
- [47] T. B ohmer, F. Pabst, J. P. Gabriel, R. Zeifler, and T. Blochowicz, On the spectral shape of the structural relaxation in supercooled liquids, *J. Chem. Phys.* **162**, 120902 (2025).
- [48] I. Pihlajamaa, C. C. L. Laudicina, and L. M. C. Janssen, Influence of polydispersity on the relaxation mechanisms of glassy liquids, *Phys. Rev. Res.* **5**, 033120 (2023).
- [49] M. P. Allen and D. J. Tildesley, *Computer Simulation of Liquids* (Oxford Science Publications (Oxford), 1987).
- [50] S. Toxvaerd and J. C. Dyre, Communication: Shifted forces in molecular dynamics, *J. Chem. Phys.* **134**, 081102 (2011).
- [51] N. K uchler and J. Horbach, Choice of diameters in a polydisperse model glassformer: Deterministic or stochastic?, *Phys. Rev. E* **106**, 064103 (2022).
- [52] N. P. Bailey, T. S. Ingebrigtsen, J. S. Hansen, A. A. Veldhorst, L. B ohling, C. A. Lemarchand, A. E. Olsen, A. K. Bacher, L. Costigliola, U. R. Pedersen, H. Larsen, J. C. Dyre, and T. B. Schr oder, RUMD: A general purpose molecular dynamics package optimized to utilize GPU hardware down to a few thousand particles, *SciPost Phys.* **3**, 038 (2017).
- [53] <https://gitlab.com/tbs.cph/rumdpy-dev> (2024).
- [54] H. Vogel, Das temperaturabhangigkeitsgesetz der viskositat von flussigkeiten, *Phys. Z.* **22**, 645 (1921).
- [55] Y. S. Elmatad, D. Chandler, and J. P. Garrahan, Corresponding states of structural glass formers, *J. Phys. Chem. B* **113**, 5563 (2009).
- [56] W. Kob and J.-L. Barrat, Aging effects in a Lennard-Jones glass, *Phys. Rev. Lett.* **78**, 4581 (1997).
- [57] T. B ohmer, J. P. Gabriel, L. Costigliola, J.-N. Kociok, T. Hecksher, J. C. Dyre, and T. Blochowicz, Time reversibility during the ageing of materials, *Nat. Phys.* **20**, 637 (2024).
- [58] D. Han, D. Wei, P.-H. Cao, Y.-J. Wang, and L.-H. Dai, Statistical complexity of potential energy landscape as a dynamic signature of the glass transition, *Phys. Rev. B* **101**, 064205 (2020).

APPENDIX

Other time-autocorrelation functions

Figures 5 and 6 show equivalents of Fig. 1 for the self-intermediate scattering function $F_s(t)$ and the first-order orientational autocorrelation function $P_1(t) = \langle \cos \Theta(t) \rangle$, respectively. Both display the same features as found for $P_2(t)$ in the main manuscript; in particular the speedup provided by Swap is identical.

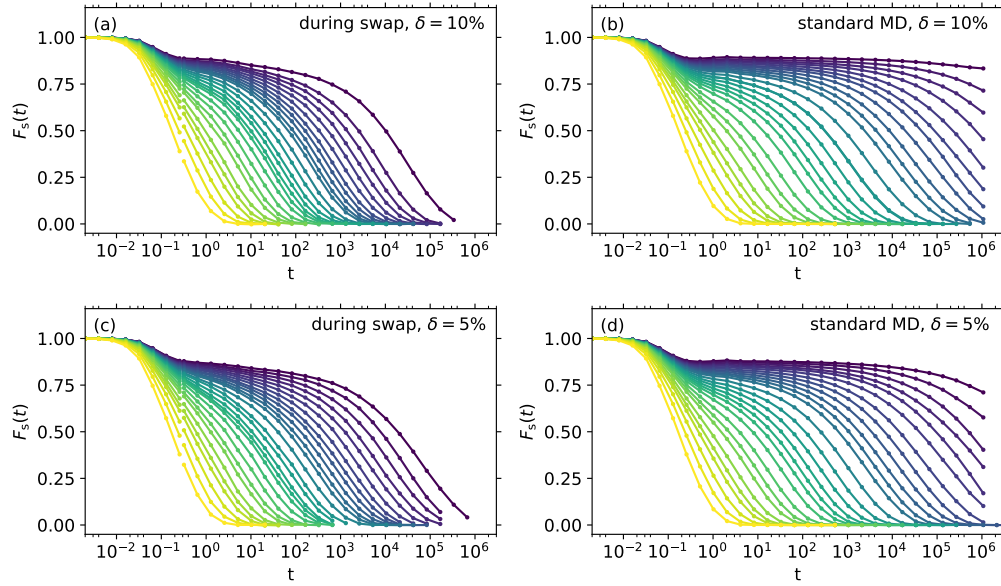


FIG. 5. Intermediate scattering function $F_s(t)$ evaluated for $q = 7.5$, approximately corresponding to the first maximum of the AA structure factor, for Swap and standard MD dynamics and the different polydispersities. For the temperature color-code see Fig. 1.

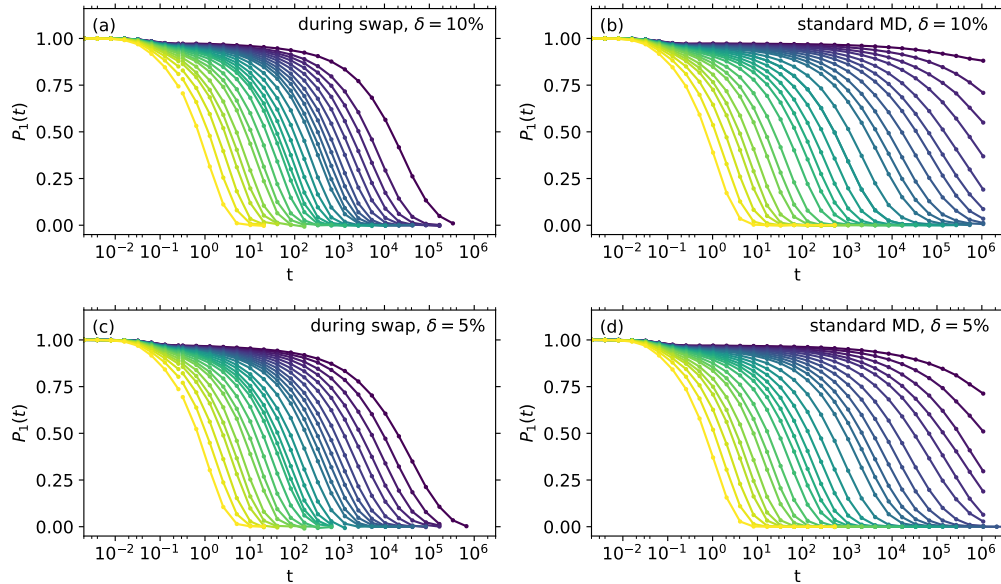


FIG. 6. First-order orientational autocorrelation function $P_1(t) = \langle \cos \Theta(t) \rangle$ for Swap and standard MD dynamics and the different polydispersities.

Swap acceptance rate

Figure 7 displays the average equilibrium acceptance rate for molecule swaps as a function of temperature for both $\delta = 5\%$ and 10% polydispersity. The values are of the same order as the acceptance rates for the standard Swap model [19, 21].

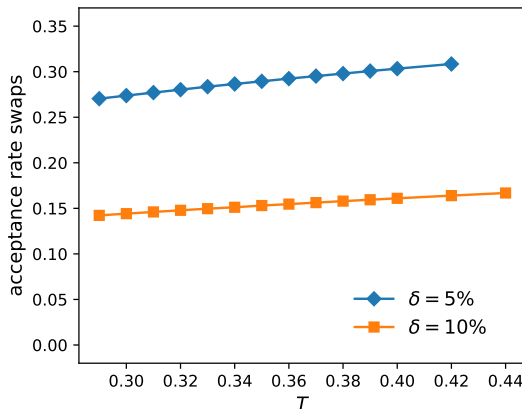


FIG. 7. Average equilibrium acceptance rate for molecule swaps as a function of temperature for both $\delta = 5\%$ and 10% polydispersity.

Removing polydispersity

Working at low polydispersities we wondered whether it might be possible to find a procedure that maps an equilibrium configurations with moderate polydispersity to an equilibrium configuration with no polydispersity. In Fig. 8 we illustrate that simply removing the polydispersity at $t = 0$ while keeping temperature constant does not yield the desired result: We observe a slow time-evolution of the average per-particle potential energy that proceeds on a time scale of the same order as τ_{MD} . At the same time is worth noticing that the observed drop in potential energy is not big, and this might be an indication that this configuration is an equilibrium configuration for the $\delta = 0\%$ at slightly higher temperature. We plan to explore this possibility in future works.

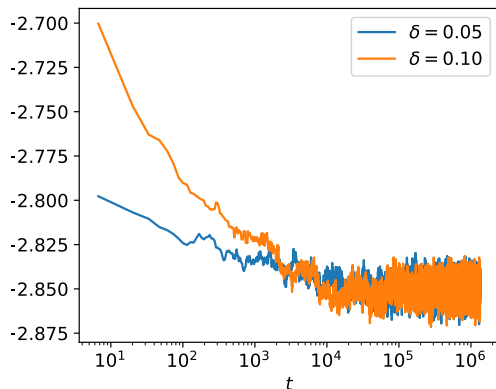


FIG. 8. Time evolution of the average per-particle potential energy after removing the polydispersity at $t = 0$ for a configuration equilibrated at $T = 0.40$.